Letter

Quantification of Ionic Diffusion in Lead Halide Perovskite Single Crystals

Wei Peng, Clara Aranda, Osman M. Bakr, Germà Garcia-Belmonte, Juan Bisquert, and Antonio Guerrero

ACS Energy Lett., **Just Accepted Manuscript** • DOI: 10.1021/acsenergylett.8b00641 • Publication Date (Web): 25 May 2018

Quantification of Ionic Diffusion in Lead Halide Perovskite Single Crystals

Wei Peng,[1,2] Clara Aranda,[1] Osman Bakr,[2*] Germà Garcia-Belmonte,[1] Juan Bisquert,[1*] Antonio Guerrero[1*]

[1] Institute of Advanced Materials (INAM), Universitat Jaume I, 12006 Castelló, Spain
[2] King Abdullah University of Science and Technology (KAUST), Division of Physical Sciences and Engineering, Thuwal 23955-6900, Kingdom of Saudi Arabia

Email: osman.bakr@kaust.edu.sa, bisquert@uji.es, aguerrer@uji.es
23 May 2018

Abstract

Lead halide perovskites are mixed electronic/ionic semiconductors that have recently revolutionized the photovoltaics field. The physical characterization of the ionic conductivity has been rather elusive due to the highly intermixing of ionic and electronic current. In this work the synthesis of low defect density monocrystalline $MAPbBr_3$ (MA=Methyl ammonium) solar cells free of hole transport layer (HTL) suppresses the effect of electronic current. Impedance spectroscopy reveals the characteristic signature of ionic diffusion (the Warburg element and transmission line equivalent circuit) and ion accumulation at the $MAPbBr_3$/Au interface. Diffusion coefficients are calculated based on a good correlation between thickness of $MAPbBr_3$ and characteristic diffusion transition frequency. In addition, reactive external interfaces are studied by comparison of polycrystalline $MAPbBr_3$ devices prepared either with or without a HTL. The low frequency response in IS measurements is correlated with the chemical reactivity of moving ions with the external interfaces and diffusion into the HTL.

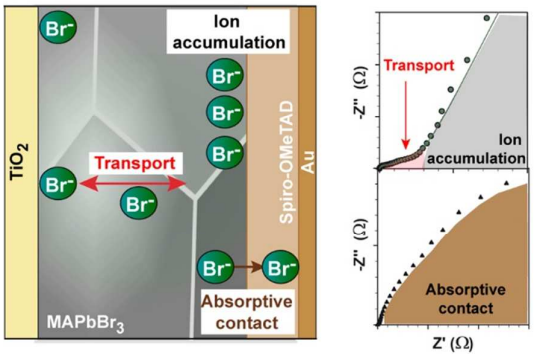

Hybrid organic-inorganic perovskite materials have revolutionized the photovoltaics field, but they are currently hampered by device performance and degradation issues that stem from a lack of understanding of their ionic conduction properties. Lead halide perovskite materials have long been known to be mixed electronic/ionic conductors[1,2] however, only recently ionic conductivity has been identified as a key player for operational mechanisms in photovoltaic devices. For example, ion migration has been related to degradation processes,[3,4] modification in the device operation mechanism affecting the extraction properties of the contacts[5,6] and inducing a hysteretic behavior during electrical operation.[7,8] Regardless of the importance of ion migration, a full characterization of the migrating species in these optically active materials has been elusive due to the highly intermixed electronic and ionic currents. In this work, high quality and low defect density monocrystalline devices of $MAPbBr_3$ have been prepared that enable direct observation of the ionic signal by suppression of the electronic current. The characteristic signature of ionic transport, ion accumulation/diffusion of ions into the external contacts is revealed by using impedance spectroscopy (IS) to investigate both high efficiency $MAPbBr_3$ monocrystalline and polycrystalline devices.

Ionic migration has been detected in lead halide perovskites by different electrical measurements in operating solar cells, such as chronoamperommetry or capacitive methods,[9,10] which provide limited amount of information. In addition, the use of ex-situ techniques has clearly confirmed the nature of the migrating species. For example, compositional imaging has been obtained using XPS[11] and time of flight secondary ion mass spectrometry (TOF-SIMS), in both cases with resolution in the z-axis direction. Robust results using the latest technique have finally clarified that the metal electrode materials and halides are the main migrating species.[4,12,13] However, none of these techniques offer kinetic information in operating devices such as the ion diffusion coefficients, which are highly valuable material parameters for evaluating the ionic conductivity properties of the material.

IS is a technique that has traditionally been used to characterize ionic transport and electrochemical reactions in a variety of devices such as batteries, dye sensitized solar cells or photoelectrochemical cells.[14-16] This technique measures the electrical response in the frequency/time domain separating resistive and capacitive contributions arising from electronic and ionic processes with different characteristic time/frequencies. In the specific case of solid state ionic diffusion, IS provides a standard and widely used method to identify the main kinetic parameters such as the chemical diffusion coefficient.[16,17] Depending on the transport properties of the materials, a transmission line can be observed in the complex impedance plot, which accounts for ionic transport in mixed ionic-electronic conductors. Furthermore, IS also provides information on the nature of boundaries and anomalous diffusion phenomena.[18,19] These methods have been previously applied to determine Li^+ ion diffusion features in lead halide perovskites,[20] but not to the displacement of intrinsic defects that are often observed to cause major effects in the photovoltaic perovskite devices. In this work, IS reveals the characteristic

signature of ionic transport in lead halide perovskite materials. High efficiency monocrystalline $MAPbBr_3$ solar cells without a hole transport layer (HTL) are an excellent model system that simplifies the electrical response. Using this method, a transmission line characteristic for ion migration is observed together with ion accumulation across the bulk perovskite layer. In addition, polycrystalline $MAPbBr_3$ devices prepared either with or without Spiro-OMeTAD enables the study of "ion-absorptive" external interfaces. It is shown that in the presence of Spiro-OMeTAD layer free bromide ions do not accumulate at the external interfaces but diffuse into the HTL as a source of chemical reactivity.

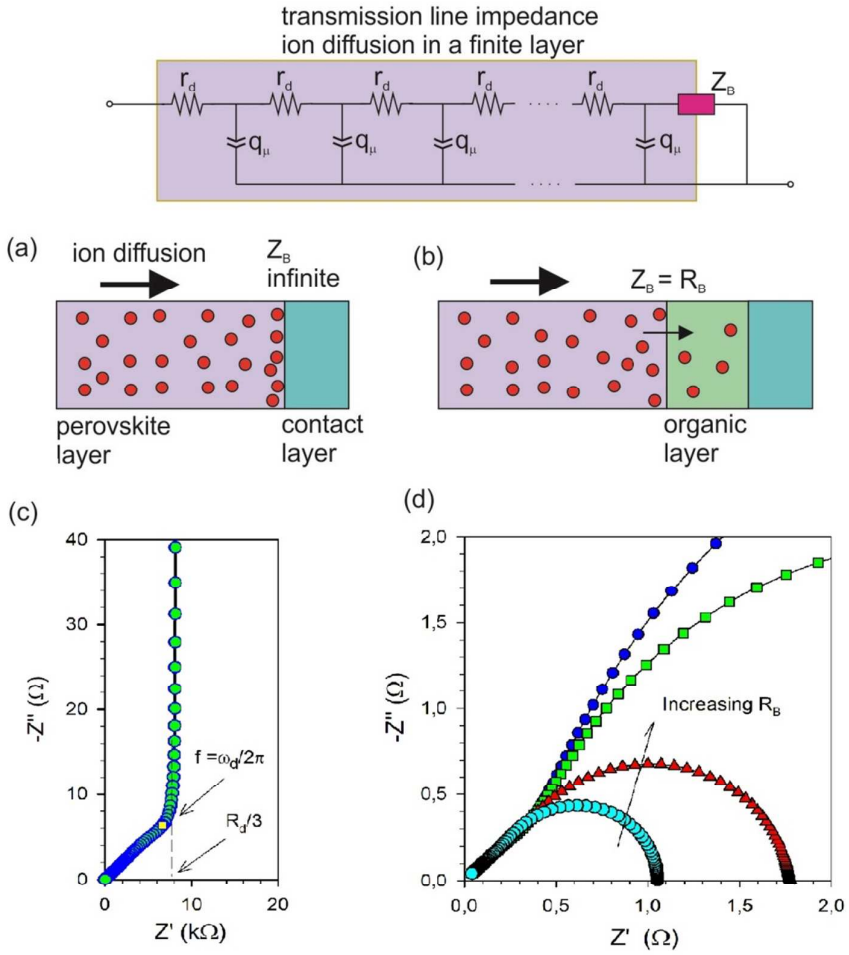

Figure 1: The impedance of ion diffusion in a finite layer is a transmission line composed of a distributed transport resistance and chemical capacitance. The process of termination at the boundary, represented by the boundary impedance, Z_B, changes dramatically the impedance spectra at low frequency. For a blocking boundary shown in (a) the impedance rises vertically (c). For a boundary that allows charge transfer (b) the impedance forms an arc at low frequency, that decreases when the charge transfer rate at the contact increases (d).

During IS measurement a dc voltage is applied to the sample under either light or dark conditions and a small-signal ac voltage perturbation is superimposed with a wide range of frequencies. The frequency and amplitude of the AC perturbation modulates how much the system is separated from equilibrium and the extent to which carriers/ions will move in the oscillating field.

The impedance of ionic diffusion in solid media has been widely applied in the context of Li ion battery materials.[15] The impedance shows two distinct features that can be obtained from the distributed equivalent circuit of a transmission line as shown in Fig. 1.[21] At high frequency the ac modulation probes the diffusion unbounded by the contacts. In this domain the representation in the complex impedance plane $(Z', -Z'')$, shows the standard Warburg element, consisting of a line with 45^{o} inclination, Fig. 1c. At low frequency there are different types of behaviors depending on the boundary conditions.[22] In the main model the final boundary is a reflecting boundary for ions which cannot enter the other medium at the contact layer, and consequently accumulate at the interface.[23] The low frequency impedance is capacitive, and it shows a vertical line associated to the ionic chemical capacitance, Fig. 1c.[24] In between the Warburg and capacitance domains of the impedance response lies the ankle of the characteristic frequency of diffusion, ω_d. When the spectrum is obtained experimentally it is quite straightforward to obtain the ionic chemical diffusion coefficient D_μ by the relation

$$\omega_d = \frac{D_\mu}{d^2} \tag{1}$$

Note that D_μ is a quantity that depends on composition.[25] However, in a highly diluted system, as expected in the low concentration of mobile defects in lead halide perovskites, the chemical diffusion coefficient should be a constant characteristic of the specific material environment of the moving ions.

Another important point is that the impedance spectroscopy will respond to the global transport properties of the system. It has been established that hybrid perovskites may contain a variety of carriers, electronic and ionic. The observation of ionic diffusion demands a specific system with a low density of electronic carriers, otherwise the ionic transport resistance will be masked by a parallel pathway of low electronic resistance. In our experimental system we have specifically addressed this issue.

In addition, it has been widely recognized that the impedance spectra can be drastically modified by the carrier boundary condition of the transport layer.[22] Systems with different contact layers are compared in Fig. 1a and b, accordingly with different specific contact boundary impedance Z_B. If the final boundary is perfectly blocking, the impedance rises in a capacitive vertical line as mentioned previously. However, for an absorptive interface that transfers or allows the diffusion of ions into a neighbor layer as occurs in Fig. 1b, an arc at low frequency will appear, Fig. 1d, with a total resistance determined by the charge transfer rate of the injection process.[18] This remark provides a useful criterion to derive the nature of the boundaries from the observed impedance spectra.[18]

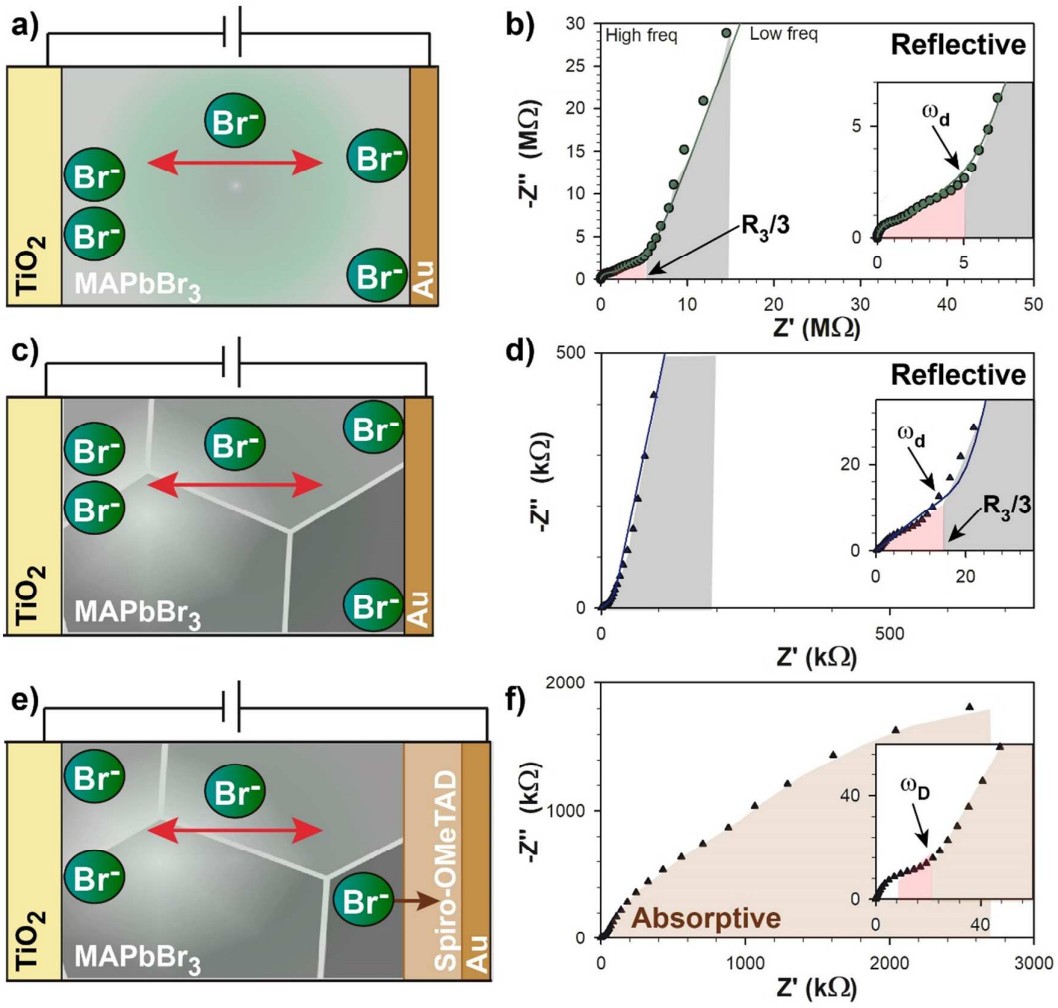

Figure 2: Different configurations used for devices containing $MAPbBr_3$: a) Monocrystalline, c) and e) Polycrystalline. b), d), f) Complex plane impedance plots extracted from impedance measures in the dark at 0 V for configurations shown on their left. Solid lines correspond to fitting results using equivalent circuit shown in Fig. 1). Ionic processes are highlighted with different colors: ionic transport (red), charge accumulation (grey) and diffusion into absorptive contacts (brown).

A series of high efficiency photovoltaic devices are prepared using either monocrystalline or polycrystalline $MAPbBr_3$. A photovoltaic configuration containing monocrystals of $MAPbBr_3$ (Fig. 2a) offers an excellent model system with low defect densities of 1.8×10^{12} cm^{-3}, see supporting information for Mott-Schottky analysis. In addition, this configuration does not contain the commonly used hole transport layer Spiro-OMeTAD simplifying the electrical response as this layer contains different additives (i.e. LiTFSI) that could lead to ion migration of additional species (i.e. Li^+).[26] Power conversion efficiencies depend on the thickness of the $MAPbBr_3$ monocrystals but are in the range of 2-5 % with a remarkably high V_{oc} close to 1.4 V, representative

photovoltaic performance data is shown as supporting information.[27] In order to study the effect of the HTL during ion migration, a polycrystalline $MAPbBr_3$ configuration is tested with and without Spiro-OMeTAD. Polycrystalline devices (Fig. 2c and 2e) have been developed in this work with improved solvent formulation leading to pinhole-free devices with an impressive morphology. Polycrystalline devices without HTL show low efficiencies of 0.3 % with photocurrent being the most affected parameter while efficiency dramatically increases to 2.0 % with the presence of Spiro-OMetad.[28] In summary mono- and polycrystalline devices are of high quality ensuring that the system is not limited by transport of electrons or holes that would ultimately lead to recombination of carriers.[29]

Monocrystalline $MAPbBr_3$ devices with different active layer thickness were measured by IS under the dark condition at 0 V (Fig. 2b). In these conditions we expect only the native mobile defects in diluted conditions so that the chemical diffusion coefficient should be the same for the different samples. The complex impedance plot clearly shows a transmission line at intermediate frequencies (red region) covering more than two orders of magnitude in the frequency scale (0.5-200 Hz). As can be observed in Fig. 2b, there is a very good agreement between the fitting results (solid lines) with the impedance data obtained for reflective boundary conditions. The aboservation of tilted lines in the low frequency range indicates anomalous diffusion patetrns as explained in the supporting information. For example, for a perovskite thickness of 1.4 micron, ω_d is 0.91 Hz and accumulation of ions at the contacts is observed at lower frequencies leading to an almost vertical line (grey region), typical for reflective contacts. The fact of observing a blocking boundary for a diode configuration indicates that the impedance for electron transport is extremely large and does not shunt the device. This feature corresponds to a sample with extremely low doping level, as reported previously.[30] This is the reason why the impedance of pure ionic diffusion can be clearly observed in these monocrystal samples.

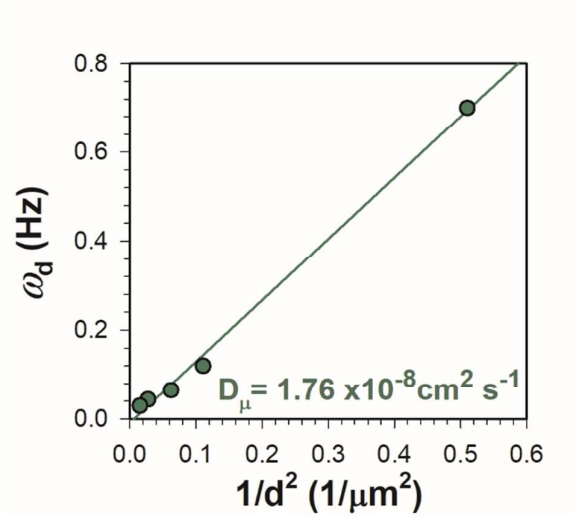

Figure 3: Dependency of characteristic frequency with the monocrystal thickness and

extracted diffusion coefficient.

As the monocrystal thickness is increased, ω_d decreases, corresponding to the increase of the transit time for ions to reach the external interfaces, according to the classical diffusion theory explained above (see Fig. 1). Very importantly, there is a balance between the ionic migration kinetics and the thickness of the sample that allows the observation of the complete transmission line pattern. For example, a monocrystal of 50 microns only shows the Warburg part and does not reveal ion accumulation at frequencies as low as 1 mHz (see supporting information). Diffusion coefficients of $D_\mu = 1.8 \times 10^{-8}$ cm^2/s can be calculated for Br^- from the correlation of the frequency of the ankle to the thickness of the perovskite layer (Fig. 2c) and using Equation (1), see Fig. 3. Note that in this device configuration there is no Spiro-OMeTAD or additives containing small ions like Li^+ which could also be transported through the perovskite matrix.[26] In addition, the large size of the methyl ammonium (MA^+) cation in comparison to the halides has been reported to be the factor why migration in $MAPbI_3$ is dominated by I^- vacancies.[31] In this work, Br^- is even smaller than the I^- analogue. For these reasons, we propose that Br^- diffusion is measured in this device configuration. It is important to highlight that migration of Br^- in monocrystalline devices is related to transport *via* vacancies/interstitial defects of the crystalline structure, not the grain boundaries. Finally, the impedance data can be fitted using the equivalent circuit described in Fig. 1.

Understanding the effect of the external interfaces is essential as highest efficiencies in photovoltaic devices are typically obtained using adequate HTL and electron transport layers (ETL). In addition, degradation processes in perovskite devices has recently been connected with reactivity at the perovskite/contact interfaces.[3,5,32] Unfortunately, using our process it is not possible to prepare monocrystalline devices with different HTL materials offering homogeneous thickness. Therefore we turn to polycrystalline $MAPbBr_3$ for comparing by IS a system free of HTL and a system containing HTL. The complex plane impedance plots are shown in Fig. 2d and 2f, respectively. At high and intermediate frequency, both HTL-free device and the sample containing Spiro-OMeTAD (Fig. 2f) show the same behavior of the crystalline system in the intermediate frequency range, corresponding to the Warburg diffusion behavior truncated to a vertical rise, see inset of Fig. 2f. However, a very different scenario is obtained at low frequencies comparing the two samples. For the HTL-free polycrystalline device a vertical line similar to that of the monocrystalline device and typical for reflective electrodes is observed. In contrast, for the Spiro-OMeTAD containing sample the low frequency line bends down as a characteristic mark of the absorbing boundary, see Fig. 1d. The fact that devices free of Spiro-OMeTAD show a reflecting boundary behavior and devices containing this HTL show a partially absorptive boundary behavior is a clear indication that Br^- diffuses into the Spiro-OMeTAD. These inserted ions can react with the oxidized HTL needed to obtain

adequate conductivity, as previously reported by us and more recently confirmed by SIMS-TOF.[5,12] We note that in many cases this type of reactivity leads to noisy signals in the frequency domain as it can take up to 16 min to measure one data point in the lowest frequency limit (1 mHz). Therefore, we can conclude that not only ions in the perovskite layer are being monitored in the transport regime but ion diffusion and reactivity with the external contacts can be monitored in real time.

In conclusion we showed that impedance spectroscopy measured in the dark provides access to the transport response of ions at intermediate frequencies providing detailed information on the diffusion coefficients. The capacitive response in the low frequency region reveals the response of ion accumulation for ion-reflective contacts, while the presence of an arc for ion-absorptive contacts supports the hypothesis for ion diffusion into the contact and/or chemical reactivity with the external interfaces. The advanced understanding presented in this study of the ionic conduction properties of this exciting type of materials open a new avenue for solving some of the main degradation and performance issues hampering perovskite optoelectronics.

Experimental Section

Monocrystalline $MAPbBr_3$ device fabrication

Monocrystalline $MAPbBr_3$ on TiO_2 (~60 nm)/FTO glass were grown using the cavitation-triggered asymmetric crystallization method, as previously reported.[27] 100 nm thick Au electrodes of full coverage on as-grown monocrystalline film were deposited through a metal shadow mask by thermal evaporation.

Polycrystalline $MAPbBr_3$ devices fabrication

$MAPbBr_3$ film was deposited on TiO_2 by spin coating at 4000 rpm for 40s, using toluene as anti-solvent. This was followed by annealing at 100 °C for 3 min to obtain a shiny and homogenous film. When required, a solution of Spiro-OMeTAD is deposited as HTL in chlorobenzene by spin coating at 4000 rpm. Finally, 60 nm of gold was thermally evaporated on top of the device as a back contact.

Film and Device characterization

Photovoltaic devices were characterized using an Abett Solar simulator equipped with 1.5 AM filter. The light intensity was adjusted to 100 $mWcm^{-2}$ using a calibrated Si solar cell. Devices were measured using a mask to define an active area of 0.11 cm^2. Impedance spectroscopy measurements were performed using an Autolab PGSTAT-30 equipped with a frequency analyzer module in the dark. The DC bias was selected at 0 V with the AC perturbation to cover the frequency range of 1 mHz to 1 MHz.

Supporting Information. Mott-Schottky analysis, Device performance characteristics, Impedance spectroscopy data, anomalous diffusion.

Acknowledgements

We acknowledge funding from Spanish Ministerio de Economía y Competitividad of

Spain under Project MAT2016-76892-C3-1-R and for a Ramón y Cajal Fellowship (RYC-2014-16809). OMB and WP acknowledge the financial support of KAUST.

References

(1) Kuku, T. A.; Salau, A. M. Electrical conductivity of $CuSnI_3$, $CuPbI_3$ and $KPbI_3$, *Solid State Ionics* **1987**, *25*, 1-7.

(2) Kuku, T. A. Ionic transport and galvanic cell discharge characteristics of $CuPbI_3$ thin films, *Thin Solid Films* **1998**, *325*, 246-250.

(3) Guerrero, A.; You, J.; Aranda, C.; Kang, Y. S.; Garcia-Belmonte, G.; Zhou, H.; Bisquert, J.; Yang, Y. Interfacial degradation of planar lead halide perovskite solar cells, *ACS Nano* **2016**, *10*, 218–224.

(4) Domanski, K.; Correa-Baena, J.-P.; Mine, N.; Nazeeruddin, M. K.; Abate, A.; Saliba, M.; Tress, W.; Hagfeldt, A.; Grätzel, M. Not all that glitters is gold: Metal-migration-induced degradation in perovskite solar cells, *ACS Nano* **2016**, *10*, 6306-6314.

(5) Carrillo, J.; Guerrero, A.; Rahimnejad, S.; Almora, O.; Zarazua, I.; Mas-Marza, E.; Bisquert, J.; Garcia-Belmonte, G. Ionic reactivity at contacts and aging of methylammonium lead triiodide perovskite solar cell *Adv. Energy Mater.* **2016**, *6*, 1502246.

(6) Xiao, Z.; Yuan, Y.; Shao, Y.; Wang, Q.; Dong, Q.; Bi, C.; Sharma, P.; Gruverman, A.; Huang, J. Giant switchable photovoltaic effect in organometal trihalide perovskite devices, *Nat. Mater.* **2015**, *14*, 193–198.

(7) Correa-Baena, J.-P.; Turren-Cruz, S.-H.; Tress, W.; Hagfeldt, A.; Aranda, C.; Shooshtari, L.; Bisquert, J.; Guerrero, A. Changes from bulk to surface recombination mechanisms between pristine and cycled perovskite solar cells, *ACS Energy Lett.* **2017**, *2*, 681-688.

(8) Tress, W.; Marinova, N.; Moehl, T.; Zakeeruddin, S. M.; Nazeeruddin, M. K.; Gratzel, M. Understanding the rate-dependent J-V hysteresis, slow time component, and aging in $CH_3NH_3PbI_3$ perovskite solar cells: the role of a compensated electric field, *Energy Environ. Sci.* **2015**, *8*, 995-1004.

(9) Lopez-Varo, P.; Jiménez-Tejada, J. A.; García-Rosell, M.; Ravishankar, S.; Garcia-Belmonte, G.; Bisquert, J.; Almora, O. Device physics of hybrid perovskite solar cells: theory and experiment. *Adv. En. Mater.* 2018, 1702772.

(10) Yang, T.-Y.; Gregori, G.; Pellet, N.; Grätzel, M.; Maier, J. The significance of ion conduction in a hybrid organic–inorganic lead-iodide-based perovskite photosensitizer, *Angew. Chem., Int. Ed.* **2015**, *54*, 7905-7910.

(11) Li, C.; Tscheuschner, S.; Paulus, F.; Hopkinson, P. E.; Kießling, J.; Köhler, A.; Vaynzof, Y.; Huettner, S. Iodine migration and its effect on hysteresis in perovskite solar cells, *Adv. Mater.* **2016**, *28*, 2446-2454.

(12) Zhang, T.; Meng, X.; Bai, Y.; Xiao, S.; Hu, C.; Yang, Y.; Chen, H.; Yang, S. Profiling the organic cation-dependent degradation of organolead halide perovskite solar cells, *J. Mat. Chem. A* **2017**, *5*, 1103-1111.

(13) Li, J.; Dong, Q.; Li, N.; Wang, L. Direct evidence of ion diffusion for the silver-electrode-induced thermal degradation of inverted perovskite solar cells, *Adv. Energy Mater.* **2017**, 1602922.

(14) Fabregat-Santiago, F.; Bisquert, J.; Palomares, E.; Otero, L.; Kuang, D.; Zakeeruddin, S. M.; Grätzel, M. Correlation between photovoltaic performance and impedance spectroscopy of dye-sensitized solar cells based on ionic liquids, *J. Phys. Chem. C* **2007**, *111*, 6550-6560.

(15) Weppner, W.; Huggins, R. A. Determination of the kinetics parameters of mixed-conducting electrodes and application to the system Li_3Sb, *J. Electrochem. Soc.* **1977**, *124*, 1569.

(16) Ho, C.; Raistrick, I. D.; Huggins, R. A. Application of a-c techniques to the study of lithium diffusion in tungsten trioxide films, *J. Electrochem. Soc.* **1980**, *127*, 343-350.

(17) Raistrick, I. D. Application of impedance spectroscopy to problems in solid state ionics, *Solid State Ionics* **1986**, *18-19*, 40.

(18) Bisquert, J. Influence of the boundaries in the impedance of porous film electrodes, *Phys. Chem. Chem. Phys.* **2000**, *2*, 4185-4192.

(19) Bisquert, J.; Compte, A. Theory of the electrochemical impedance of anomalous diffusion, *J. Electroanalytical Chem.* **2001**, *499*, 112-120.

(20) Vicente, N.; Garcia-Belmonte, G. Organohalide perovskites are fast ionic conductors, *Adv. Energy Mater.* **2017**, *7*, 1700710.

(21) Bisquert, J.; Fabregat-Santiago, F. Impedance Spectroscopy: A general introduction and application to dye-sensitized solar cells; Kalyanasundaram, K., Ed.; CRC Press: Boca Raton, 2010.

(22) Bisquert, J.; Garcia-Belmonte, G.; Bueno, P. R.; Longo, E.; Bulhões, L. O. S. Impedance of constant phase element (CPE) -blocked diffusion in film electrodes, *J. Electroanalytical Chem.* **1998**, *452*, 229-234.

(23) García-Rosell, M.; Bou, A.; Jiménez-Tejada, J. A.; Bisquert, J.; Lopez-Varo, P. Analysis of the influence of selective contact heterojunctions on the performance of perovskite solar cells, *J. Phys. Chem. C* **2018**, 10.1021/acs.jpcc.1028b01070.

(24) Bisquert, J. *Nanostructured Energy Devices: Equilibrium Concepts and Kinetics*;

CRC Press: Boca Raton, 2014.

(25) Bisquert, J. *Nanostructured Energy Devices: Foundations of carrier Transport*; CRC Press: Boca Raton, 2017.

(26) Li, Z.; Xiao, C.; Yang, Y.; Harvey, S. P.; Kim, D. H.; Christians, J. A.; Yang, M.; Schulz, P.; Nanayakkara, S. U.; Jiang, C.-S. *et al*. Extrinsic ion migration in perovskite solar cells, *Energy Environ. Sci.* **2017**, *10*, 1234-1242.

(27) Peng, W.; Wang, L.; Murali, B.; Ho, K.-T.; Bera, A.; Cho, N.; Kang, C.-F.; Burlakov, V. M.; Pan, J.; Sinatra, L. *et al.* Solution-grown monocrystalline hybrid perovskite films for hole-transporter-free solar cells, *Adv. Mater.* **2016**, *28*, 3383-3390.

(28) Arora, N.; Orlandi, S.; Dar, M. I.; Aghazada, S.; Jacopin, G.; Cavazzini, M.; Mosconi, E.; Gratia, P.; De Angelis, F.; Pozzi, G. *et al.* High open-circuit voltage: Fabrication of formamidinium lead bromide perovskite solar cells using fluorene–dithiophene derivatives as hole-transporting materials, *ACS Energy Lett.* **2016**, *1*, 107-112.

(29) Gonzalez-Pedro, V.; Juarez-Perez, E. J.; Arsyad, W.-S.; Barea, E. M.; Fabregat-Santiago, F.; Mora-Sero, I.; Bisquert, J. General working principles of $CH_3NH_3PbX_3$ perovskite solar cells, *Nano Lett.* **2014**, *14*, 888-893.

(30) Shi, D.; Adinolfi, V.; Comin, R.; Yuan, M.; Alarousu, E.; Buin, A.; Chen, Y.; Hoogland, S.; Rothenberger, A.; Katsiev, K. *et al.* Low trap-state density and long carrier diffusion in organolead trihalide perovskite single crystals, *Science* **2015**, *347*, 519-522.

(31) Azpiroz, J. M.; Mosconi, E.; Bisquert, J.; De Angelis, F. Defect migration in methylammonium lead iodide and its role in perovskite solar cell operation, *Energy Environ. Sci.* **2015**, *8*, 2118--2127.

(32) Hou, Y.; Du, X.; Scheiner, S.; McMeekin, D. P.; Wang, Z.; Li, N.; Killian, M. S.; Chen, H.; Richter, M.; Levchuk, I. *et al.* generic interface to reduce the efficiency-stability-cost gap of perovskite solar cells, *Science* **2017**, *358*, 1192-1197.